

## Numerical study of 10-year-old child forearm injury

Haojie Mao<sup>\*a</sup>, Yun Cai and King H. Yang

*Department of Biomedical Engineering, Wayne State University*

*(Received September 05, 2013, Revised February 14, 2014, Accepted June 23, 2014)*

**Abstract.** Forearm fractures in children are very common among all pediatric fractures. However, biomechanical investigations on the pediatric forearm are rather scarce, partially due to the complex anatomy, closely situated, interrelated structures, highly dynamic movement patterns, and lack of appropriate tools. The purpose of this study is to develop a computational tool for child forearm investigation and characterize the mechanical responses of a backward fall using the computational model. A three-dimensional 10-year-old child forearm finite element (FE) model, which includes the ulna, radius, carpal bones, metacarpals, phalanges, cartilages and ligaments, was developed. The high-quality hexahedral FE meshes were created using a multi-block approach to ensure computational accuracy. The material properties of the FE model were obtained by scaling reported adult experimental data. The design of computational experiments was performed to investigate material sensitivity and the effects of relevant parameters in backward fall. Numerical results provided a spectrum of child forearm responses with various effective masses and forearm angles. In addition, a conceptual L-shape wrist guard design was simulated and found to be able to reduce child distal radius fracture.

**Keywords:** pediatric forearm fractures; finite element model; pediatric biomechanics; parametric study; wrist guard design

---

### 1. Introduction

There are approximately 1.4 million estimated cases of hand/forearm fractures each year in the United States, accounting for 1.5% of all emergency department cases (Chung and Spilson 2001). Distal radius and carpal fractures in children and adolescents account for approximately 25% of all pediatric fractures (de Putter *et al.* 2011). The age group of 5 to 14 years old comprises the largest proportion (26%) of all hand and forearm fractures than any other age groups (de Putter *et al.* 2011). Radius and/or ulna fractures take up the largest proportion of fractures (32.9%) in age group 5 to 14 years old. A population-based study revealed that the incidence rate of forearm fractures in boys and girls in this age group increased dramatically. In particular, the age group 10 to 14 have the highest increase in the period from 1997 to 2009 (de Putter *et al.* 2011).

The pediatric musculoskeletal system is distinctly different from that of an adult. Although these differences decrease with age, they present unique injury patterns and challenges in the diagnosis and treatment of pediatric orthopedic problems. Pediatric bone is highly cellular and

---

\*Corresponding author, Ph.D, E-mail: haojie.mao@gmail.com

<sup>a</sup>Current affiliation: Research Scientist at DoD Biotechnology HPC Software Application Institute (BHS AI)

porous, and it contains much more collagen and cartilage compared with adult bone. The abundance of collagen leads to a reduction of tensile strength and prevents the propagation of fractures, whereas the large amount of cartilage enhances resilience (Carson *et al.* 2006). The young bone has great ability to undergo large plastic deformation as opposed to limited plastic deformation in adult. Consequently, the strain tolerance of young bone is higher (Currey and Butler 1975). Even though, the incidence rate of pediatric forearm fracture is still higher, because for children, anything the mind can conceive and the hand can reach is likely to be tried. When accident happens, the hand is the body part most often thrust out to lessen the consequence, resulting in a wide array of hand injuries (Beatty *et al.* 1990). The wrist bones consist of eight irregular shape bones: scaphoid, lunate, pisiform, triquetrum, trapezium, trapezoid, capitate and hamate. The pisiform does not appear on radiographs until 9 or 10 years of age (Carson *et al.* 2006).

Pediatric forearm fractures have been described in several studies, but the proportion of fractures in these studies is controversial (Carson *et al.* 2006, Parmelee-Peters and Eathorne 2005). For example, Parmelee-Peters *et al.* (2005) indicated that scaphoid fractures are the most common in the age 15 to 30 years and are rare under the age of 10, whereas Carson *et al.* (2006) pointed out that as in adults, the scaphoid fracture is the most common fracture in children. Further biomechanical analysis to investigate the pediatric forearm responses is warranted.

The primary methods of studying human injury mechanisms are biomechanical experiments and computational simulations. Due to ethical and legal concerns, pediatric cadavers are rarely used for biomechanical experiments. As an alternative, animals are used as surrogates to study pediatric injury biomechanics. For instance, Koo *et al.* (2001) determined the correlation between noninvasive bone mass measurement and bone strength using swine. However, using animal is challenging because of different growth stages. In addition, the anatomical structures and tissue properties of a child are significantly different from those of animal. It is difficult to correlate injury mechanisms in children and those in animal. The finite element (FE) method is an effective way to investigate injury mechanism, which can provide child-specific biomechanical response at tissue level.

Currently, no pediatric forearm FE model has been reported in literature specifically related to impact biomechanics. For the adult, Carrigan *et al.* (2003) developed an adult carpal model from CT scans. This model adopted detailed stiffness value of each ligament. Gislason *et al.* (2010) developed an adult wrist model from MRI scans. Javanmardian and HaghPanahi (2010) developed an adult wrist model from CT scans. Guo *et al.* (2009) developed a wrist FE model to study the procedure of transecting the transverse carpal ligament. Bajuri *et al.* (2013) used a FE model to analyze the biomechanics of wrist arthroplasty. These efforts demonstrated benefits and potential of using FE modeling to advance wrist/hand biomechanics study.

The majority of wrist injuries are consequences of falls. Distal radius fractures on the outstretched arms/hands were observed in both backward and forward falls (Schmitt *et al.* 2012). Several studies have indicated that the risk of sustaining wrist fractures can be decreased by wearing a wrist guard (Lewis *et al.* 1997, Machold *et al.* 2002). To ensure a minimum level of protection, quantification of relevant parameters is required which include the effective mass, impact angle, and impact velocity (drop height). In this study, a three-dimensional 10-year-old child forearm FE model, consisting of the ulna, radius, carpal bones, metacarpals, phalanges, cartilages and ligaments, was developed to characterize mechanical responses of backward fall. The effects of effective mass and angle were studied. Additionally, a conceptual wrist guard FE model was created to mitigate distal radius fractures.

## 2. Methods

The baseline geometry was scaled from an adult FE model guided by published radiologic images (Godderidge 1995). The scale factors for a 10-year-old child were  $\lambda_x = 0.647$ ;  $\lambda_y = 0.647$ ;  $\lambda_z = 0.787$  (Mertz *et al.* 2001), along the anteroposterior, lateral-medial, and distal-proximal direction, respectively. All parameters were first scaled uniformly, and then locally adjusted based on the measurements taken from children in the age range of 9-11 years old (Mao *et al.*, 2014). A multi-block approach was used in this study to create high quality hexahedral meshes for the main part of the forearm using ANSYS ICEM CFD/HEXA 12.0 (Ansys, Canonsburg, PA, USA). Hypermesh 10.0 (Altair, Troy, MI) was used to generate the rest of the meshes and improve mesh qualities manually.

### 2.1 Material Modeling

Both cortical and cancellous bones were modeled as isotropic elastic-plastic material using a piecewise-linear-plasticity material (MAT 24) in LS-DYNA. The cancellous bone was modeled using hexahedral elements while shell elements were used to represent the cortical bone. Cartilages were modeled as isotropic elastic material (MAT 1), using quadrilateral elements. Currently, there is no report about pediatric forearm material properties. Ivarsson *et al.* (2013) provided extensive review of the biomechanical data for pediatric extremities and pelvis, no data on hand/wrist was reported. In the adult, the reported Young's modulus ranged typically from 10 to 18GPa for cortical bones, 100MPa for cancellous bones, and 10MPa for cartilages (Table 1) (Carrigan *et al.* 2003). According to Mertz *et al.* (2001), the scale factor of the elastic modulus for a 10-year-old child relative to a midsize male is 0.854. Material laws and properties assumed for the 10-year-old child forearm model are summarized in Table 2. Ligaments only provide tension resistance. An elastic tension only bar element (MAT 74) was used to simulate ligaments (Table 3), because ligaments only provide tension resistance (Table 3). Phalanges were treated as rigid (MAT 20), as most fractures caused in falls are distal radius fractures.

According to Carson *et al.* (2006), the carpus is composed entirely of cartilage at birth and remains predominantly cartilaginous until the late childhood and adolescent years. As a result, mechanisms that would produce bony wrist injuries in the mature skeleton produce fractures of the forearm bones in young children. The capitate is the first carpal bone to begin ossification at 2 to 3 months of age, and the hamate closely follows approximately 1 month later. Ossification then proceeds in a clockwise manner. The triquetrum begins to ossify at 2 years of age, the lunate ossifies at age 3, the scaphoid ossifies at age 5, and the trapezoid and trapezium ossify at age 6. The pisiform does not appear on radiographs until 9 or 10 years of age. Based on these descriptions, the growth plate of carpal bones was not represented.

### 2.2 Mesh Convergence Study

Details of the mesh convergence study are described in Appendix section. Basically, mesh convergence was studied using the radius model in a simulated perpendicular impact to a rigid plate along the gravitational direction (Z-direction) with an impact velocity of 2.8 m/s. Elements from different areas were chosen to depict the relationship between the calculated von Mises stress and mesh size. Five levels of mesh size were studied. The largest mesh size was 4.8 mm. The mesh size was reduced to 3.2, 2.4, 1.6, and 0.8 mm using the multi-block approach. Since the

Table 1 List of several reported material parameter for adult

Part	Material type	Material parameters	Reference
Cartilage	linear elastic	E=5MPa, Nu=0.49	Miyake <i>et al.</i> 1994
Bone	linear elastic	Cortical, E=15GPa, Nu=0.3	
	Elastic-plastic	Cancellous, E=100MPa, Nu=0.2	
Cartilage	linear elastic	E=10MPa, Nu=0.45	Carrigan <i>et al.</i> 2003
Bone	linear elastic	E=10GPa, Nu=0.3	
Cartilage	linear elastic	E=10MPa, Nu=0.45	Anderson <i>et al.</i> 2005
Bone	Linear elastic isotropic	Cortical, E=13.8GPa, Nu=0.3	
	Linear elastic isotropic	Cancellous, E=1400MPa, 690MPa, and 345MPa, Nu=0.3	
Cartilage	Hyperelastic, Mooney-Rivlin	C10=4.1MPa, C01=0.41MPa, Rho=1.1 g/cm <sup>3</sup>	Gislason <i>et al.</i> 2010
Bone	linear elastic	Cortical, E=18GPa, Nu=0.2, Rho=2.0 g/cm <sup>3</sup>	
	linear elastic	Cancellous, E=100MPa, Nu=0.25, Rho=1.3 g/cm <sup>3</sup>	
Cartilage	linear elastic	E=10MPa, Nu=0.45	Javanmardian and HaghPanahi 2010
Bone	linear elastic	E=10GPa, Nu=0.3	

distal radius was the part that contacted and impacted the plate, elements in different regions of the radius were picked for the convergence study. Based on the analysis, a typical spatial resolution of 1-3.2 mm was chosen to capture detailed anatomical structures within current computational capabilities. For the carpal bones, because of their irregular shape and small geometry size, the mesh sizes were set around 1.5 mm. In total, the model consists of 10,510 hexahedral, 7,430 shell elements, and 173 bar elements (Fig. 1). The quality of the mesh for the 10-year-old child forearm model is listed in Table 4.

### 2.3 Computational Simulation

Greenwald *et al.* (1998) dropped twelve adult cadaveric arms sectioned below the elbow from a height of 0.4 m. Each of the forearms was mounted on a drop complex with an effective mass of 23.0 kg. This mass was chosen because it corresponded to 1/3 of the body mass of an average adult, representing the portion of the upper body that would be directly above the arm in a backward fall. Each forearm was positioned at an angle of 75° with respect to the force platform. The wrists of each specimen were positioned in about 40° of dorsiflexion and 10° of internal rotation (pronation). This particular wrist angle was a likely orientation of an unbraced wrist before a fall. Using the law of energy conservation, the vertical velocity of the drop complex at impact was estimated to be 2.8 m/s.

Table 2 Material properties assumed for the 10-year-old forearm model and the scale factors used to determine properties

Part	Element type	Material type	Material parameters	Scale factor (References)
Cartilage	Quadrilateral	Isotropic elastic	E=8.54MPa, Nu=0.45	
Carpal bones, Cortical	Quadrilateral	Isotropic elastic-plastic	E=15.4GPa, Nu=0.2, Yield=179 MPa	
Carpal bones, Cancellous	Hexahedral	Isotropic elastic-plastic	E=85.4MPa, Nu=0.25, Yield=5.6 MPa	
Matecarpals, Cortical	Quadrilateral	Isotropic elastic-plastic	E=15.4GPa, Nu=0.2, Yield=179 MPa	
Matecarpals, Cancellous	Hexahedral	Isotropic elastic-plastic	E=85.4MPa, Nu=0.25, Yield=5.6 MPa	0.854 (Irwin and J., 1997, Mertz <i>et al.</i> 2001)
Radius, Cortical	Quadrilateral	Isotropic elastic-plastic	E=8.64GPa, Nu=0.2, Yield=64.1 MPa	
Radius, Cancellous	Hexahedral	Isotropic elastic-plastic	E=300MPa, Nu=0.3, Yield=3 MPa	
Ulna, Cortical	Quadrilateral	Isotropic elastic-plastic	E=8.64GPa, Nu=0.2, Yield=64.1 MPa	
Ulna, Cancellous	Hexahedral	Isotropic elastic-plastic	E=300MPa, Nu=0.3, Yield=3 MPa	

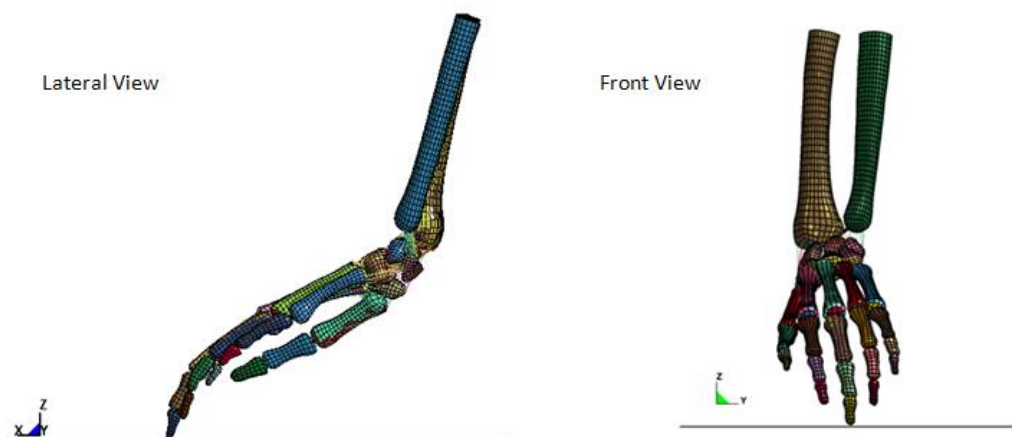


Fig. 1 The 10-year-old child forearm FE model. FE: finite element

Table 3 List of assumed ligament stiffness

Ligament	Material type	Stiffness specified (N/mm)	Scale factor (Reference)
Pisohamate Ligament		25.6	
Ligaments of metacarpals		921.6	
Radial Collateral Ligament		34.16	
Pisometacarpal Ligament		51.3	
Palmar Radiocarpal Ligaments		260	0.854
Palmar Intercarpal Ligaments	Elastic spring discrete beam (tensile only)	444.6	(Irwin and J., 1997, Mertz <i>et al.</i> 2001)
Dorsal Radiocarpal Ligament		266.5	
Dorsal Intercarpal Ligament		359.1	
Carpometacarpal Ligaments		265.2	
Palmar Ulnocarpal Ligaments		153.9	
Palmar Carpo-metacarpal Ligament		363.8	

The 10-year-old forearm model was rotated to the same angles as those in Greenwald's cadaveric experiments. An effective mass of 10.8 kg, approximately 1/3 of the body mass of an average 10-year-old child, was added to the proximal end of the radius and ulna and the impact velocity was assumed to be 2.8 m/s to simulate a fall from 0.4 m. The proximal end of the radius was allowed to move in vertical direction and fixed in other two degrees of freedom, representing laboratory experimental settings (Greenwald *et al.* 1998). The contacts between the plate and full hand were defined to represent the physical condition with frictionless penalty-based surface-to-surface contacts. That being said, based on the current setting in which the fingers were in the lowest position, the plate comes into contact with finger first, followed by carpal bones and distal radius. The simulations were performed and analyzed using LS-DYNA 971 (LSTC, Livermore, CA) MPP version.

Table 4 Qualities of the 10-year-old child forearm mesh

Element type	Jacobian		Warpage		Skew		Aspect ratio		Quad face minimum angle		Quad face maximum angle	
Solid	≥0.4	Min.	≤50	Max.	≤60	Max.	≤5	Max.	≥30	Min.	≤150	Max.
	99.1%	0.34	99.0%	58.3	100%	58.4	100%	5.0	99.9%	28.1	99.1%	159.7
Shell	≥0.5	Min.	≤30	Max.	≤30	Max.	≤3	Max.	≥45	Min.	≤135	Max.
	99.3%	0.48	98.5%	49.3	98.6%	55.6	99.8%	3.3	99.2%	30.4	98.6%	156.5

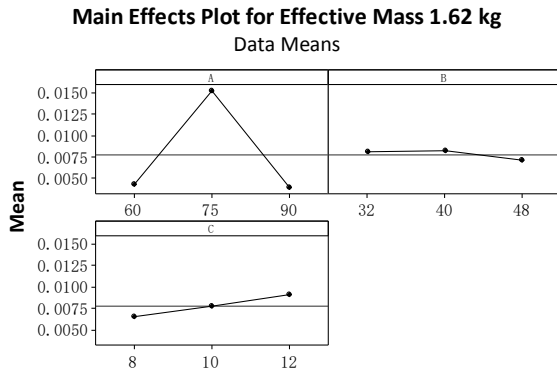


Fig. 2 1.62 kg case\*

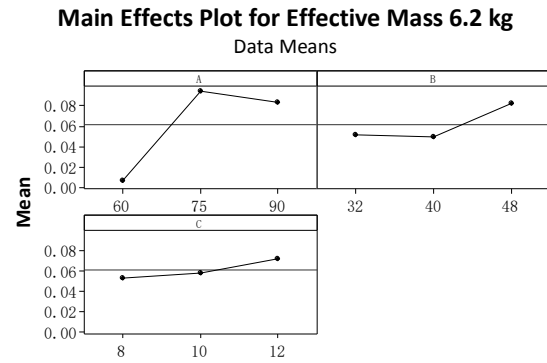


Fig. 3 6.2 kg case\*

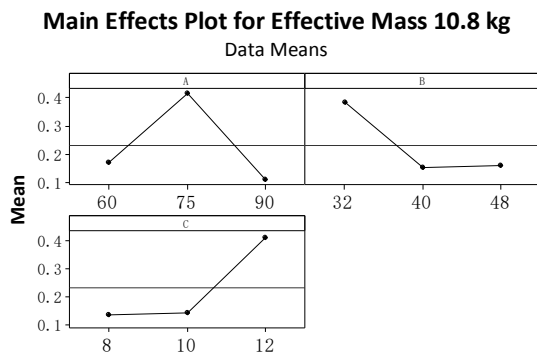


Fig. 4 10.8 kg case\*

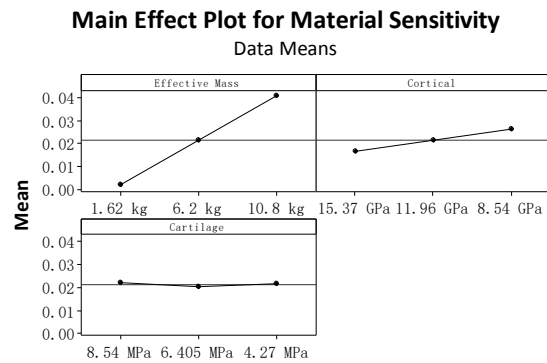


Fig. 5 Sensitivity study\*

\* A is the angle between forearm and platform, B is the angle of dorsiflexion, and C is the angle of internal rotation. For Fig. 2, 3, and 4, the abscissa is the magnitude of the angle and the ordinate is the MPS. MPS: maximum principal strain.

### 2.4 Design of Computer Experiments (DOCE)

Design of experiments (DOE) has been widely employed to study the effect of multiple variables with multiple factors simultaneously. Nowadays, the same concept is expanded to numerical simulations to investigate the effect of different factors such as those affecting brain injuries (Mao *et al.* 2010b). Based on a literature review, three parameters defining the mechanical responses of backward falls were identified: the effective mass, impact angle, and impact velocity (related to drop height). Schmitt *et al.* (2012) reviewed several studies and reported that the lowest reported effective mass was about 5% of an adult body weight. In the current computational simulation, three different effective masses were tested: 10.8 kg (Greenwald *et al.* (1998), about 1/3 of total body weight of 10-year-old child), 1.62 kg (5% of total body weight of 10-year-old child), and 6.2 kg (the average of the aforementioned effective masses).

The average maximum ranges of motion at the wrist are 59 degrees for extension, 79 degrees for flexion, 21 degrees of radial deviation, and 38 degrees of ulna deviation (Werner and Plancher

1998). Three relevant angles were analyzed in this study: the angle between forearm and platform (impact angle), angle of dorsiflexion, and angle of internal rotation (pronation) (Greenwald *et al.* 1998). The ranges of these angles were set as  $75\pm 15$ ,  $40\pm 8$  and  $10\pm 2$  degrees, correspondingly. A four-factor (effective mass and the above three angles), three-level, full factorial DOCE analysis was designed, for a total of 81 cases, in order to systematically evaluate the effect of effective mass and angles on the risk of distal radius fractures.

Additionally, the effect of different material properties was also studied. The upper and lower bounds for the cortical bone were 15.37GPa and 8.54GPa, respectively, while the upper and lower bounds for cartilages were 8.54MPa and 4.27MPa, respectively (Table 1). A three-factor (effective mass, cortical bone modulus, cartilage modulus), three-level, full factorial analysis was simulated for a total 27 cases. The DOCE and analysis of results were performed using Minitab (Ver. 15.0, State College, PA).

### 3. Results

The maximum principal strain (MPS) for cortical bone of the distal radius was calculated in all cases and listed in Table 5. Based on the literature (Lindahl and Lindgren 1967, Takahashi *et al.* 2000), the ultimate strain of cortical bone for adult is from 2.0% to 3.0%. Jiang *et al.* (2014) estimated a scale factor for the failure strain for a 10-year-old child to be 1.3. Assuming 3.9% is the fracture threshold, an effective mass of 1.62 kg resulted in no risk of distal radius fracture. When the effective mass is 6.2 kg, the estimated fracture risk is 40.7% while the risk increases to 96.3% when the effective mass is 10.8 kg.

Factorial analysis for effective mass 1.62 kg (part A in Fig. 2), in the form of a main effect chart, indicated that a 75-degree angle between the forearm and platform has the highest average MPS. The angle of dorsiflexion has little effect in all simulations (part B in Fig. 2) and the MPS increases linearly with the internal rotation angle (part C in Fig. 2). Main effect analysis for an effective mass of 6.2 kg (Fig. 3) and 10.8 kg (Fig. 4) demonstrated that all three angles have a non-linear effect on the MPS and when the angle between forearm and platform is 75 degrees, the effect for the MPS is the highest.

For the material sensitivity study, increasing the effective mass corresponds to a linear increase in MPS (Fig. 5). As expected, increasing the Young's modulus of cartilage has little effect on the MPS but an increase in the Young's modulus of cortical bones reduced the cortical MPS.

### 4. Discussion

This study established a stable numerical FE model that can be used to predict forearm injuries of a 10-year-old child. In turn, the model can be used to design safety countermeasures. To the best of the authors' knowledge, no experimental data on 10-year-old pediatric subjects have been reported, thus comparisons between experiments and simulations for model validation were not feasible. The material properties were obtained by scaling down from adult FE models and experimental data. The scale factors were based on literatures.

The effective mass is intended to apply a similar inertial load to the forearm, as would the inertial loading from the mass of the upper arm and body. The DOCE results indicated that the effective mass has substantial effect on the model-predicted MPS, which agrees with the physics.

Table 5 Model-predicted maximum principal strain for 81 DOCE cases. Note: A is the angle between forearm and platform, B is the angle of dorsiflexion and C is the angle of internal rotation

A	B	C	Maximum principal strain		
			1.62 kg	6.2 kg	10.8 kg
90	48	8	0.0031	0.0819	0.1053
90	48	12	0.0071	0.1203	0.0797
90	32	10	0.0028	0.1038	0.1293
90	32	8	0.0024	0.0962	0.0965
60	40	8	0.0037	0.0054	0.1775
60	48	12	0.0034	0.0061	0.2735
90	40	10	0.0029	0.0570	0.1325
60	40	10	0.0051	0.0071	0.1830
75	32	12	0.0084	0.1207	2.582
60	40	12	0.0056	0.0084	0.2505
90	40	8	0.0031	0.0627	0.1157
75	32	10	0.0238	0.0095	0.0897
75	40	12	0.0386	0.1193	0.1751
75	48	10	0.0133	0.2014	0.2458
60	32	10	0.0066	0.0045	0.1313
60	32	8	0.0032	0.0059	0.1533
75	40	10	0.0026	0.0331	0.0594
60	48	8	0.0031	0.0032	0.1559
60	32	12	0.0031	0.0059	0.0151
75	32	8	0.0202	0.0096	0.1559
60	48	10	0.0039	0.0058	0.1927
75	48	8	0.0104	0.0831	0.1043
75	48	12	0.0108	0.1407	0.1413
90	32	12	0.0023	0.1033	0.1095
90	40	12	0.0030	0.0242	0.0920
90	48	10	0.0085	0.0996	0.1204
75	40	8	0.0092	0.1296	0.1845

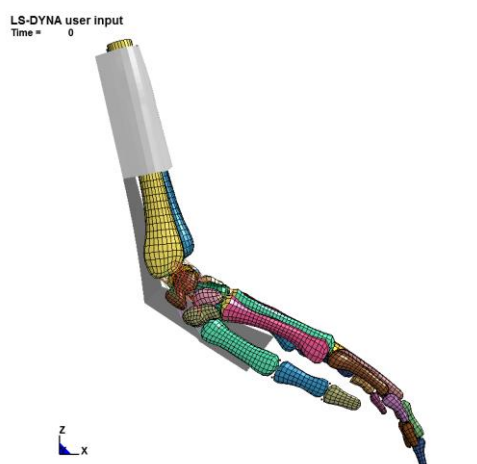


Fig. 6 Conceptual L-shape wrist guard

However, in real-world cases, it is hard to change the effective mass during a fall. In this study, an effective mass of 10.8 kg at an impact velocity of 2.8 m/s resulted in a 96.4% fracture risk. Training children to land softly and transfer the impact forces help to reduce effective mass, as such, reduce injury risk.

In addition, the angle between the forearm and platform (part A in Figs. 2-4) has similar effect for the three effective masses. At 75 degrees, all three effective masses induce the highest MPS. The MPS increases as the internal rotation angle (part C in Figs. 2-4) increases. No trend can be found for the dorsiflexion angle.

There are two basic concepts when designing a wrist guard: energy absorption and shunting. Using the concept of shunting, a conceptual L-Shape wrist guard was designed to transmit part of the impact energy to the mid-shaft (Fig. 6). The wrist guard and the lower arm model were defined with tied contacts. Comparing Figs. 7 (baseline) and 8 (with wrist guard), it can be seen that the area with high stress in the distal radius region was much smaller with a wrist guard while the area for the high stress in the radius shaft increased when a wrist guard was simulated. Because a mid-shaft radius fracture is much easier to treat and fewer medical complications compared to a distal radius fracture, a design based on shunting may become a temporary fix until a better energy-absorbing wrist guard can be designed to eliminate distal radius fracture. Moreover, Schmitt *et al.* (2011) analyzed the impact behavior of lists of commercial sport wrist protectors. Two kinds of experiment were achieved: drop test, which analyzed the damping behavior of product to protect the palm of the hand, and bending test, which characterized the stiffness of a protector to prevent hyperextension (Schmitt *et al.* 2011). In the future work, the same tests are warranted for children to more comprehensively analyze the behavior of the designed wrist guard.

There are several limitations in this study. The primary one is related to the material properties and experimental data. As there were no suitable cadaveric test data obtained from pediatric specimens, a scaling method was used to represent the material properties for the child model. The accuracy of the scale factors selected as well as the extent of model validation cannot be ascertained. We adopted penalty-based contacts that provided compressive resistances while allowing sliding motions, which represented high flexibility of a child wrist. For adult wrist model, Gislason *et al.* (2010) preferred kinematic contact algorithm to the penalty contact for additional

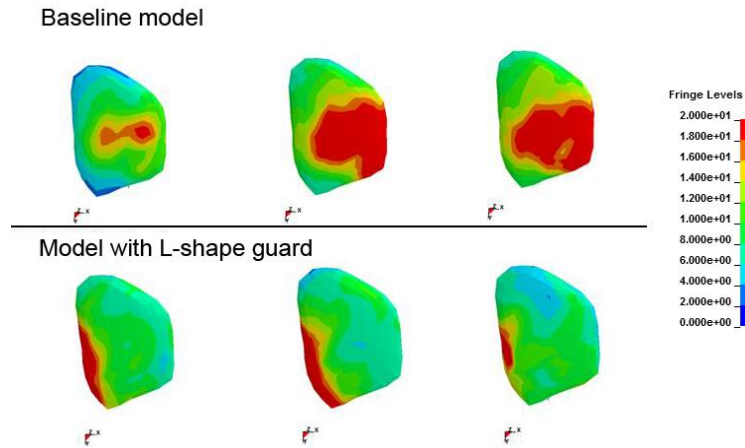


Fig. 7 Comparison of stress contours of distal radius for models with and without wrist guard, the unit for stress is MPa

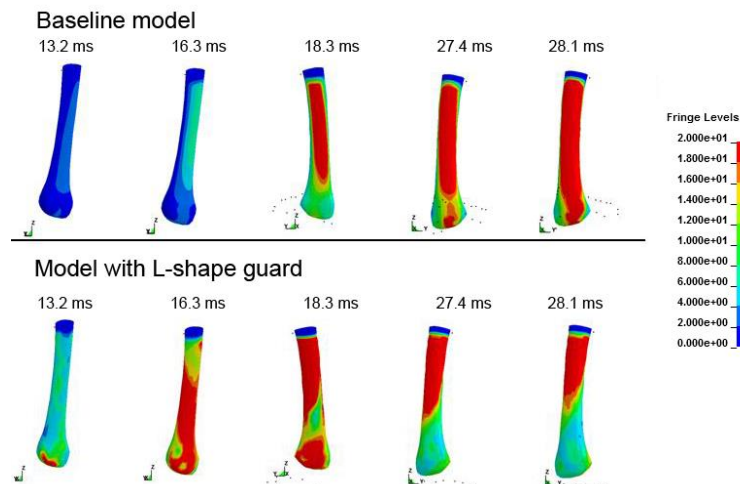


Fig. 8 Comparison of stress contours of radius shaft for models with and without wrist guard, the unit for stress is MPa

stiffness to the system. No validation of carpal bone contacts was feasible due to the lack of pediatric experimental data. In addition, the existent model could be further improved with more accurate positioning of bones and ligaments based on higher resolution medical images to be collected in the future. The ligament materials could be improved by incorporating rate-sensitive characteristics. The mesh convergence study was performed on a single radius bone instead of the complex forearm model. Similar approach of using simple model instead of complex model for mesh density studies has been used for traumatic brain injury study (Mao *et al.* 2010a). Nevertheless, despite these limitations, the pediatric forearm model provided stress distributions of child radius under lower back fall under various boundary conditions and evaluated the effect of a wrist guard design.

Although different loading conditions were considered in the computational simulations, the multi-axial loading that most likely occurs in a real-world backward fall was not simulated. In addition, this FE model does not contain the full arm, which means the rotation of elbow was not included. Since the angle of elbow plays a very important role during the fall, future research is suggested to include the elbow. Finally, the model does not contain muscle; this might be one of the reasons for the high strain value observed in simulations. It is recommended to develop a full arm model with muscles to simulate multi-axial fall loading in the future.

## 5. Conclusions

A systematic computational design of experiments for the 10-year-old forearm was performed. The mesh sizes between 1 and 3.2 mm are suitable and reasonable for the current FE model. Besides the effective mass, the impact angles and forearm internal angles were found to affect the mechanical response of a backward fall. An energy-shunting wrist guard was found to effectively alter the high stress area from the distal radius to mid-shaft.

## Acknowledgments

Toyota's Collaborative Safety Research Center (CSRC) funded Wayne State Bioengineering Center for the 10-year-old finite element model development.

## References

- Anderson, D.D., Deshpande, B.R., Daniel, T.E., Baratz, M.E., (2005), "A three-dimensional finite element model of the radiocarpal joint: distal radius fracture step-off and stress transfer", *Iowa Orthop. J.*, **25**, 108-117.
- Bajuri, M.N., Abdul Kadir, M.R., Murali, M.R., Kamarul, T., (2013), "Biomechanical analysis of the wrist arthroplasty in rheumatoid arthritis: a finite element analysis", *Med. Biol. Eng. Comput.*, **51**(1-2), 175-186.
- Beatty, E., Light, T.R., Belsole, R.J., Ogden, J.A., (1990), "Wrist and hand skeletal injuries in children", *Hand Clin.*, **6**(4), 723-738.
- Carrigan, S.D., Whiteside, R.A., Pichora, D.R., Small, C.F., (2003), "Development of a three-dimensional finite element model for carpal load transmission in a static neutral posture", *Ann. Biomed. Eng.*, **31**(6), 718-725.
- Carson, S., Woolridge, D.P., Colletti, J., Kilgore, K., (2006), "Pediatric upper extremity injuries", *Pediatr. Clin. North. Am.*, **53**(1), 41-67.
- Chung, K.C., Spilson, S.V., (2001), "The frequency and epidemiology of hand and forearm fractures in the United States", *J. Hand Surg. Am.*, **26**(5), 908-915.
- Currey, J.D., Butler, G., (1975), "The mechanical properties of bone tissue in children", *J. Bone Joint Surg. Am.*, **57**(6), 810-814.
- de Putter, C.E., van Beeck, E.F., Looman, C.W., Toet, H., Hovius, S.E., Selles, R.W., (2011), "Trends in wrist fractures in children and adolescents, 1997-2009", *J. Hand Surg. Am.*, **36**(11), 1810-1815.
- Gislason, M.K., Stansfield, B., Nash, D.H., (2010), "Finite element model creation and stability considerations of complex biological articulation: The human wrist joint", *Med. Eng. Phys.*, **32**(5), 523-531.
- Godderidge, C., (1995), "Pediatric Imaging", Saunders, Philadelphia, USA.

- Greenwald, R.M., Janes, P.C., Swanson, S.C., McDonald, T.R., (1998), "Dynamic impact response of human cadaveric forearms using a wrist brace", *Am. J. Sports Med.*, **26**(6), 825-830.
- Guo, X., Fan, Y., Li, Z.M., (2009), "Effects of dividing the transverse carpal ligament on the mechanical behavior of the carpal bones under axial compressive load: a finite element study", *Med. Eng. Phys.*, **31**(2), 188-194.
- Irwin, A., Mertz, H., (1997), Biomechanical basis for the CRABI and hybrid III child dummies. *SAE Technical Paper 973317*, doi:10.4271/973317.
- Ivarsson, J., Okamoto, M., Takahashi, Y., (2013), *Experimental Injury Biomechanics of the Pediatric Extremities and Pelvis*. Springer, New York, USA.
- Javanmardian, A., HaghPanahi, M., (2010), "Three dimensional finite element analysis of the human wrist joint without ligaments under compressive loads", *6th World Congress of Biomechanics (WCB 2010). August 1-6, 2010 Singapore IFMBE Proceedings* **31**, 628-631.
- Jiang, B., Cao, L., Mao, H., Wagner, C., Marek, S., Yang, K.H., (2014), "Development of a 10-year-old paediatric thorax finite element model validated against cardiopulmonary resuscitation data", *Comput. Methods Biomech. Biomed. Engin.*, **17**(11), 1185-1197.
- Koo, M.W., Yang, K.H., Begeman, P., Hammami, M., Koo, W.W., (2001), "Prediction of bone strength in growing animals using noninvasive bone mass measurements", *Calcif. Tissue Int.*, **68**(4), 230-234.
- Lewis, L.M., West, O.C., Standeven, J., Jarvis, H.E., (1997). "Do wrist guards protect against fractures?", *Ann. Emerg. Med.*, **29**(6), 766-769.
- Lindahl, O., Lindgren, A.G., (1967), "Cortical bone in man. II. Variation in tensile strength with age and sex", *Acta Orthop. Scand.*, **38**(2), 141-147.
- Machold, W., Kwasny, O., Eisenhardt, P., Kolonja, A., Bauer, E., Lehr, S., Mayr, W., Fuchs, M., (2002), "Reduction of severe wrist injuries in snowboarding by an optimized wrist protection device: a prospective randomized trial", *J. Trauma*, **52**(3), 517-520.
- Mao, H., Jin, X., Zhang, L., Yang, K.H., Igarashi, T., Noble-Haeusslein, L.J., King, A.I., (2010a), "Finite element analysis of controlled cortical impact-induced cell loss", *J. Neurotrauma*, **27**(5), 877-888.
- Mao, H., Yang, K.H., King, A.I., Yang, K., (2010b), "Computational neurotrauma-design, simulation, and analysis of controlled cortical impact model", *Biomech. Model Mechanobiol.*, **9**(6), 763-772.
- Mao, H., Holcombe, S., Shen, M., Jin, X., Wagner, C.D., Wang, S.C., Yang, K.H., and King, A.I., (2014), "Development of a 10-year-old full body geometric dataset for computational modeling", *Ann. Biomed. Eng.*, **42**(10), 2143-2145.
- Mertz, H.J., Jarrett, K., Moss, S., Salloum, M., Zhao, Y., (2001), "The Hybrid III 10-Year-Old Dummy", *Stapp. Car Crash J.*, **45**, 319-328.
- Miyake, T., Hashizume, H., Inoue, H., Shi, Q., Nagayama, N., (1994), "Malunited Colles' fracture. analysis of stress distribution", *J. Hand Surg. Br.*, **19**(6), 737-742.
- Parmelee-Peters, K., Eathorne, S.W., (2005), "The wrist: common injuries and management", *Prim. Care*, **32**(1), 35-70.
- Schmitt, K.U., Michel, F.I., Staudigl, F., (2011), "Analysing the impact behaviour of recent snowboarding wrist protectors", *Proc. Proceedings of the 2011 International IRCOBI Conference on the Biomechanics of Injury*, 51-61.
- Schmitt, K.U., Wider, D., Michel, F.I., Brugger, O., Gerber, H., Denoth, J., (2012), "Characterizing the mechanical parameters of forward and backward falls as experienced in snowboarding", *Sports Biomech.*, **11**(1), 57-72.
- Takahashi, Y., Kikuchi, Y., Konosu, A., Ishikawa, H., (2000), "Development and validation of the finite element model for the human lower limb of pedestrians", *Stapp. Car Crash J.*, **44**, 335-355.
- Werner, S.L., Plancher, K.D., (1998), "Biomechanics of wrist injuries in sports", *Clin. Sports Med.*, **17**(3), 407-420.

## Appendix

Fig. A2 shows the calculated von Mises stresses for elements located in the distal central region (Fig. A1). It can be seen that the stress-time histories predicted by a mesh size of 1.6, 2.4, and 3.2 mm were similar in magnitude. Similarly, Fig. A3 and A4 show that stresses predicted using these three mesh sizes are fairly consistent for the lower and upper regions of the distal radius. Figure A5 shows the elements selected near the mid-shaft and proximal end of the radius for comparison of von Mises stress as a function of mesh size. For models with mesh density 0.8 to 3.2 mm, two adjacent elements were selected for one specific region. In general, stress-time histories for five models were consistent (Figs. A6 and A7).

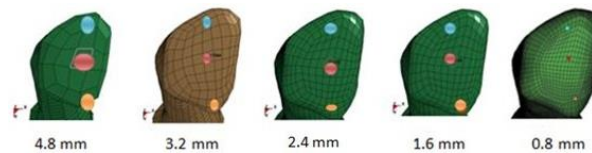


Fig. A1 The five mesh sizes for convergence study and the areas chosen for comparison of von Mises stress\*  
 \* Red circle indicates the center elements chosen for comparison of von Mises stress, Yellow circle shows the lower portion elements chosen for comparison of von Mises stress, and Blue circle represents the upper portion element chosen for comparison of von Mises stress

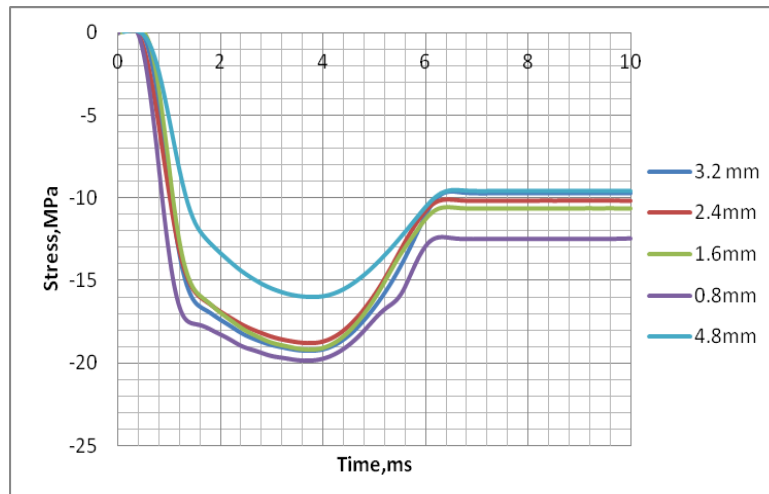


Fig. A2. Calculated von Mises stress time histories for center elements of the radius chosen for comparisons

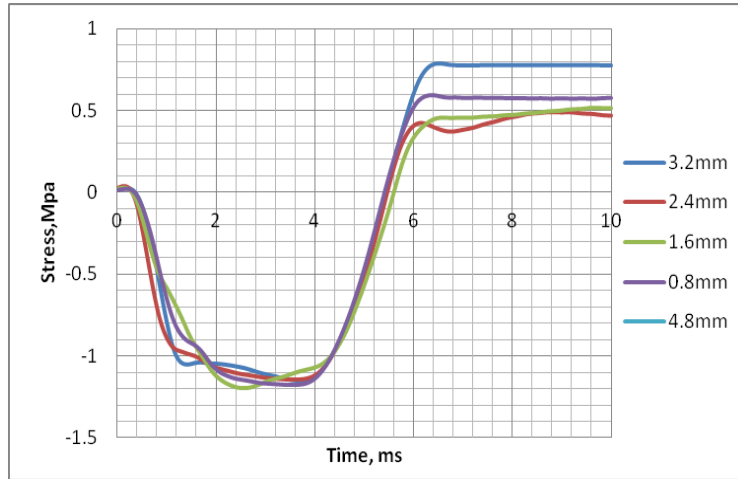


Fig. A3 Calculated von Mises stress time histories for elements in the lower distal radius chosen for comparisons

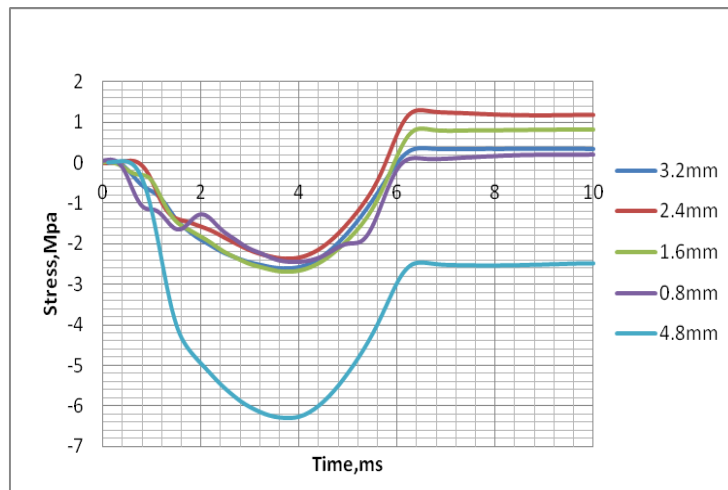


Fig. A4 Calculated von Mises stress time histories for elements in the upper distal radius chosen for comparisons

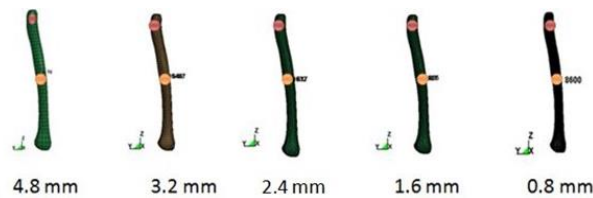


Fig. A5. The areas chosen in the radius for comparison of von Mises stress\*

\* The yellow circle presents the elements chosen in radius shaft and the red circle shows the elements in proximal end of radius chosen for comparison of von Mises stress.

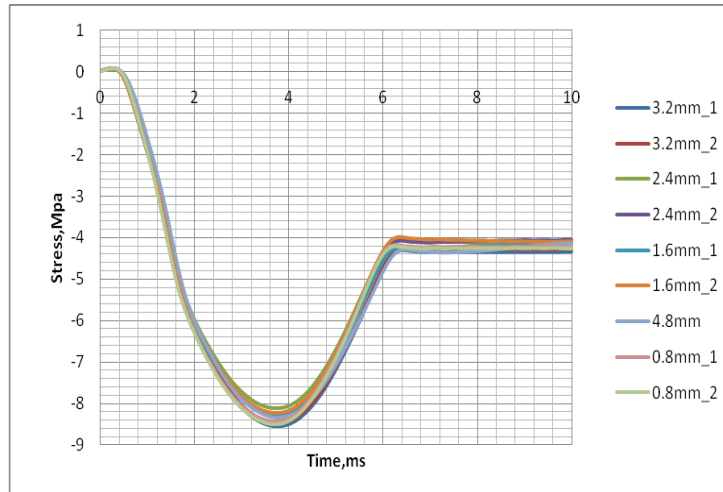


Fig. A6 Calculated von Mises stress time histories for elements in the mid shaft of the radius chosen for comparisons

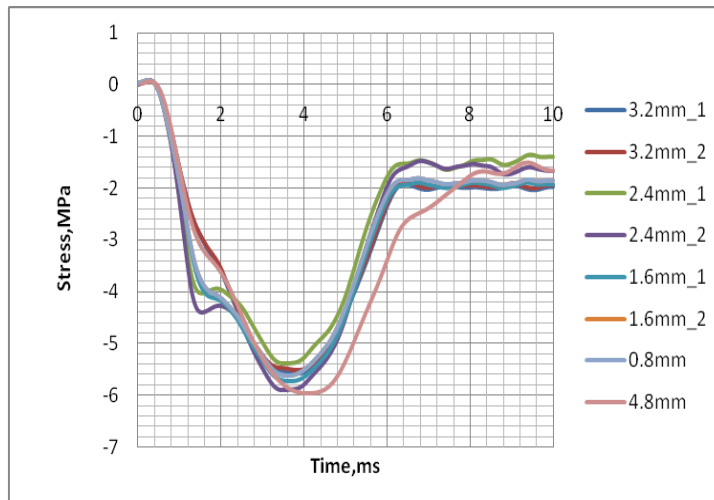


Fig. A7 Calculated von Mises stress time histories for elements in the proximal end of the radius chosen for comparisons